Electronic Supplementary Material (ESI) for Chemical Science.

Supporting Information

Sequence-Independent Activation of Photocycloadditions Using Two Colours of Light

Philipp Kamm,[abc] Leona L. Rodrigues,[ab] Sarah L. Walden,[ab] James P. Blinco,*[ab] Andreas-Neil Unterreiner,*[c] and Christopher Barner-Kowollik*[ab]

a Centre for Materials Science, Queensland University of Technology (QUT), 2 George Street, Brisbane, QLD 4000, Australia.

b School of Chemistry and Physics, Queensland University of Technology (QUT), 2 George Street, Brisbane, QLD 4000, Australia.

c Molecular Physical Chemistry Group, Institute of Physical Chemistry, Karlsruhe Institute of Technology (KIT), Fritz-Haber-Weg 2, Geb. 30.44, 76131 Karlsruhe, Germany.

Contents

1 SUPPORTING FIGURES

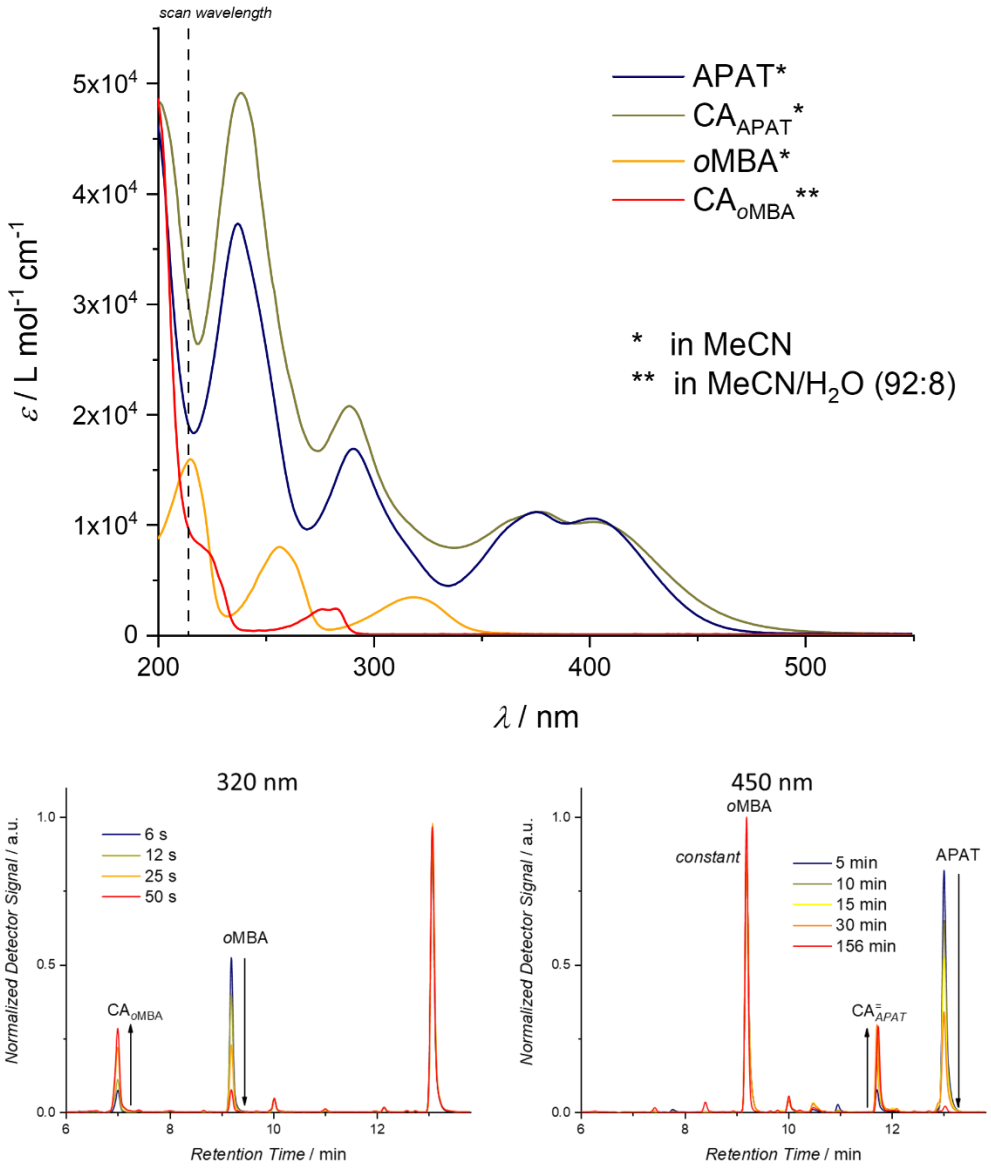

Figure S 1 Top: Absorption spectra of all investigated species. All spectra were recorded in 1 cm quartz cells, and the solvent composition was according to the gradient on the column (pure MeCN for all species except CA_{oMBA}, which was measured in a MeCN/H_2O mixture (92:8). Bottom: Exemplary chromatograms after irradiation with laser light at different wavelengths and times. At 320 nm, exclusively *o*MBA is converted. At 450 nm, exclusively APAT is converted. After 156 min of 450 nm irradiation, a number of minor side products occur, which could not be identified.

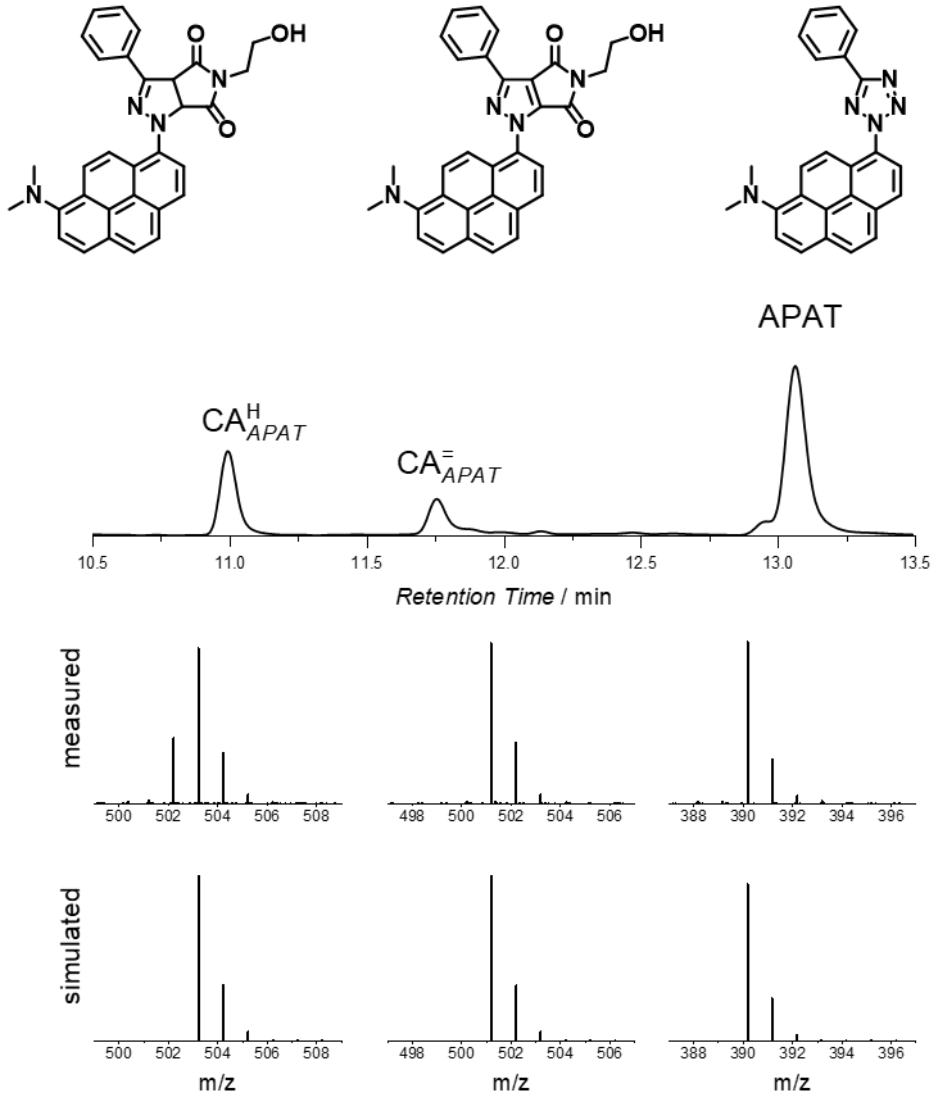

Figure S 2 Exemplary LC-MS chromatogram after LED irradiation at 445 nm. Zoom into the mass spectra corresponding to each chromatogram peak. Left peak: non-rearomatized pyrazoline adduct $\mathrm{CA}^{\mathrm{H}}_{APAT}$. $[M+H]^+$ = 503.2078. Found: 503.2076 (Δm/z = 0.4 ppm). Non-protonated species $[M]^+$ is found as well. Middle peak: rearomatized pyrazole-adduct $\mathrm{CA}^{=}_{APAT}$. $[M+H]^+$ = 501.1921. Found: 501.1928 (Δm/z = 1.4 ppm). Right peak: APAT. [M+H] = 390.1713. Found: 390.1717 (Δm/z = 1.0 ppm).

Interestingly, the non-rearomatized pyrazoline-adduct was observed exclusively in the LED experiments, where the rubber septum was penetrated repeatedly to withdraw samples, and likely traces of oxygen and moisture were present. During the laser experiments, however, full rearomatization took place and no pyrazoline-cycloadduct was found.

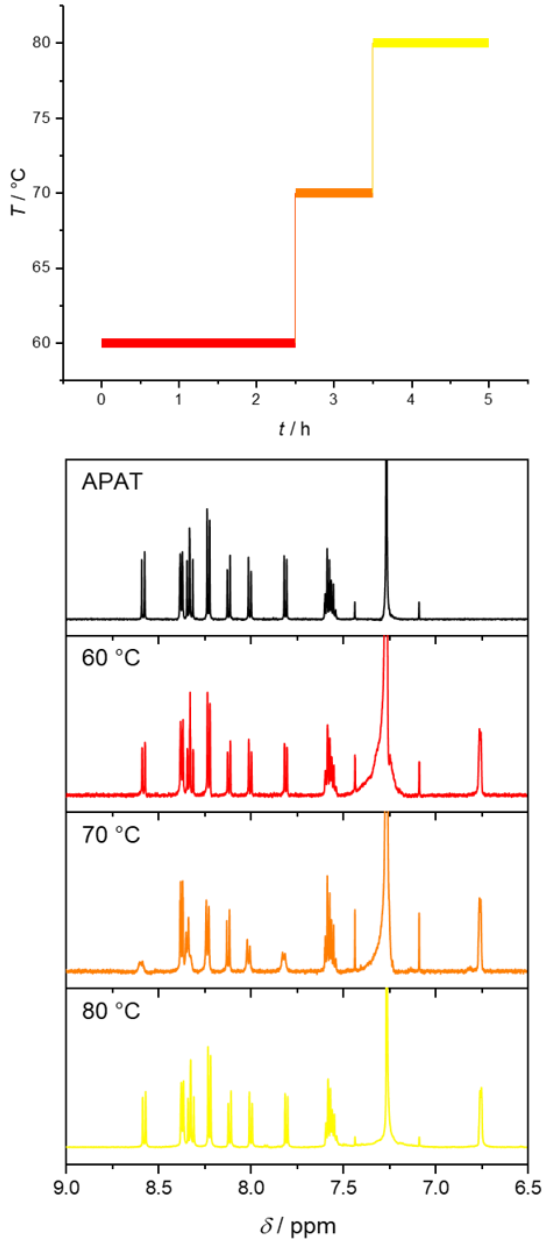

Figure S 3 Testing of the temperature-stability of APAT. A mixture of APAT and maleimide end-capped PMMA in MeCN was heated to 60 °C for 2.5 h, then 70 °C for 1 h, and then 80 °C for another 1.5 h. Samples were withdrawn and measured in $CDCl_3$ at ambient temperature. For clarity, only the characteristic aromatic region of the ^{1}H-NMR spectra is shown. The signal at 6.55 corresponds to the vinylic protons of maleimide. No change of signals was detected in the ^{1}H-NMR spectra, indicating that APAT is stable at T ≤ 80 °C, which is close to the solvent boiling point. Therefore, we rule out thermal formation of the nitrile imine. This is consistent with literature, which states that tetrazoles are temperature-stable up to ~160-220 °C. [1]

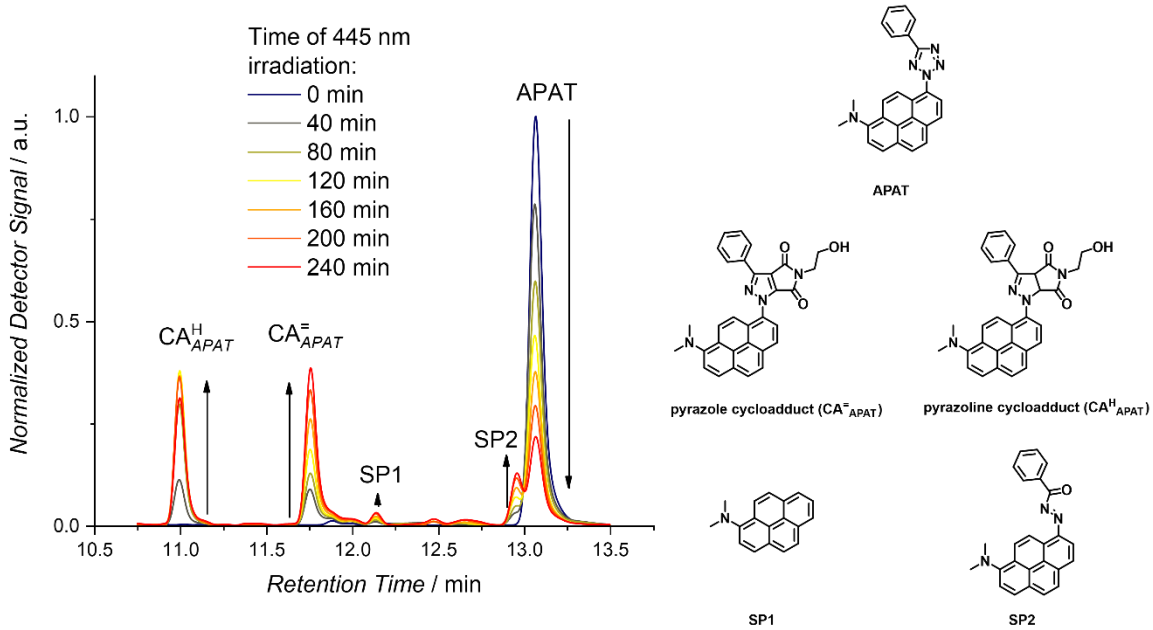

Figure S 4 Progress of APAT photoreaction in the LED experiment. Unlike in the laser experiments, varying but significant amounts of the non-rearomatized pyrazoline-cycloadduct CA^{H}_{APAT} are formed. Furthermore, trace amounts of a side-product SP1 are present, but do not correlate with irradiation time. We assume it is an impurification in the starting material of APAT. Moreover, significant amounts of SP2 are formed. The overall amount of SP2 at the end of the experiment is ~10 %.

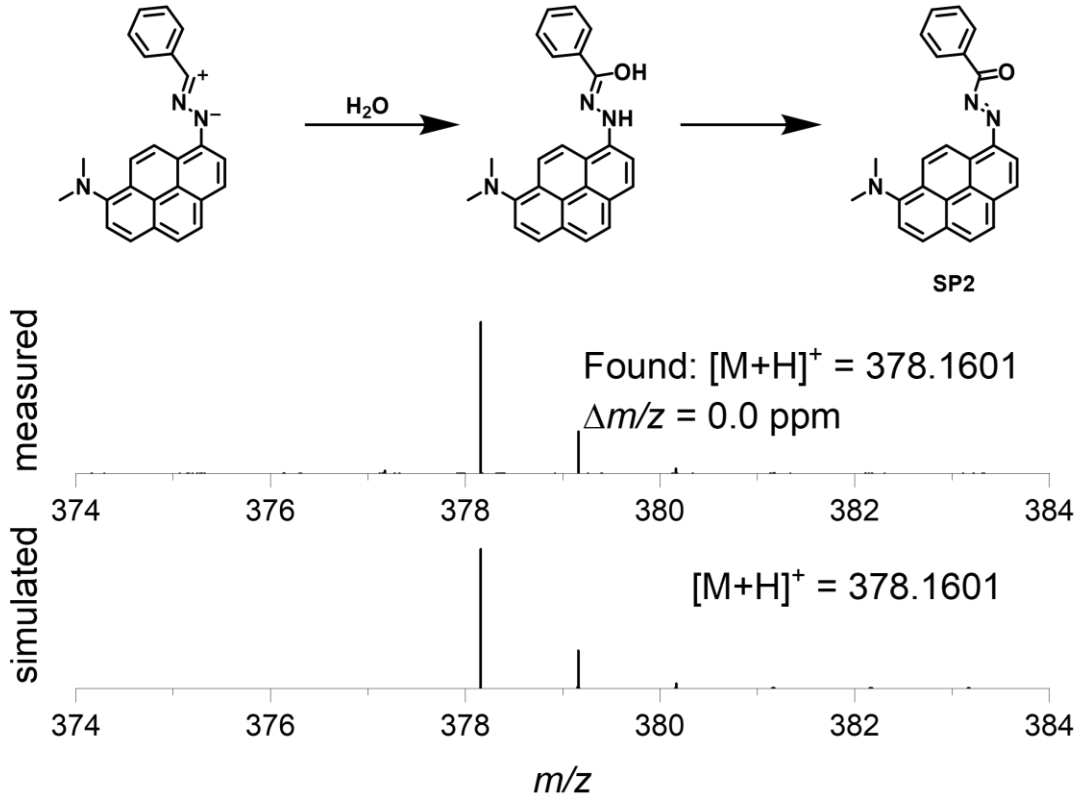

Figure S 5 1,3-dipolar cycloaddition of the nitrile imine with water, forming a hydrazonic acid intermediate, which undergoes tautomerization to the hydrazide and then form the diazo derivative.[2]

2 Methods and Instrumentation

2.1 Characterization Instruments

2.1.1 Nuclear Magnetic Resonance (NMR) spectroscopy

^{1}H-NMR, ^{13}C-NMR as well as DEPT 135, COSY, HSQC and HMBC-spectra were recorded on a Bruker System 600 Ascend LH, equipped with a BBO-Probe (5 mm) with z-gradient (^{1}H: 600.13 MHz, ^{13}C 150.90 MHz). Resonances are reported in parts per million (ppm) relative to tetramethylsilane (TMS). The δ-scale was calibrated to the respective solvent signal of $CHCl_3$ or DMSO for ^{1}H spectra and for ^{13}C spectra on the middle signal of the $CDCl_3$ triplet or the DMSO quintet. The annotation of the signals is based on HSQC-, COSY- and DEPT-experiments.

2.1.2 Liquid Chromatography Coupled Mass Spectrometry (LC-MS)

Liquid-chromatography coupled mass spectrometry (LC-MS) measurements were performed on an UltiMate 3000 UHPLC System (Dionex, Sunnyvale, CA, USA) consisting of a pump (LPG 3400SZ), autosampler (WPS 3000TSL) and a temperature-controlled column compartment (TCC 3000). Separation was performed on a C18 HPLC column (Phenomenex Luna 5µm, 100 Å, 250 × 2.0 mm) operating at 40 °C. A gradient of acetonitrile:H_2O 5:95 to 100:0 (v/v) in 7 min at a flow rate of 1.0 mL min^{-1} was applied. The flow was split in a 9:1 ratio, where 90 % of the eluent was directed through a DAD UV-detector (VWD 3400, Dionex) and 10 % was infused into the electrospray source. Spectra were recorded on an LTQ Orbitrap Elite mass spectrometer (Thermo Fisher Scientific, San Jose, CA, USA) equipped with a HESI II probe. The instrument was calibrated in the m/z range 74-1822 using premixed calibration solutions (Thermo Scientific). A constant spray voltage of 3.5 kV, a dimensionless sheath gas and a dimensionless auxiliary gas flow rate of 5 and 2 were applied, respectively. The capillary temperature and was set to 300 °C, the S-lens RF level was set to 68, and the aux gas heater temperature was set to 100 °C. Samples were prepared at concentration of 0.5 mg mL^{-1} in MeCN and filtered through 0.22 µm PTFE membrane filters prior to injection.

2.1.3 Chromatography

Flash chromatography was performed on a *Interchim* XS420+ flash chromatography system consisting of a SP-in-line filter 20-µm, an UV-VIS detector (200-800 nm) and a *SofTA* Model 400 ELSD (55 °C drift tube temperature, 25 °C spray chamber temperature, filter 5, EDR gain mode) connected via a flow splitter (*Interchim* Split ELSD F04590). The separations were performed using a *Interchim* dry load column (liquid injection) and a *Interchim* Puriflash Silica HP 30 µm column or *Interchim* Puriflash Silica HP 15 µm column (where indicated).

2.1.4 UV/VIS SPECTROSCOPY

UV-Vis spectra were recorded on a Shimadzu UV-2700 spectrophotometer equipped with a CPS-100 electronic temperature control cell positioner. Samples were prepared in solvent MeCN or MeCN/H2O mixture and measured in 10 mm Hellma Analytics quartz high precision cells at 25 °C. Molar absorption coefficients were obtained by measuring spectra at various concentrations and applying Beer-Lambert's law to calculate a linear fit:

$$OD = \varepsilon * d * c \qquad (2-1)$$

2.2 PHOTOCHEMICAL PROCEDURES

2.2.1 LASER EXPERIMENTS

2.2.1.1 LASER SETUP

All laser experiments were conducted using a *Coherent Opolette* 355 tuneable OPO, operated at wavelengths between 320 nm and 450 nm with a full width half maximum of 7 ns and a repetition rate of 20 Hz. The emitted pulse, which has a flat-top spatial profile, was expanded to 6 mm diameter using focussing lenses and directed upwards using a prism. The spectral linewidth (FWHM) of the beam is 4-6 cm^{-1}. The energy of the laser pulses was downregulated by an attenuator (polarizer). The beam was redirected into the vertical cylindrical hole of a custom-made sample holder, which contains the samples during the experiments (**Figure S 6**). These glass vials were crimped 0.7 mL vials by LLG Labware, Lab Logistic Group GmbH (Art. Nr. 4-008202). The energy of the incident laser pulses was measured by an Energy Max PC power meter (Coherent) directly above the sample holder (before the sample was inserted into the sample holder). Prism and sample holder are positioned in a way that the complete diameter of the hole of the sample holder was covered by the incident laser beam.

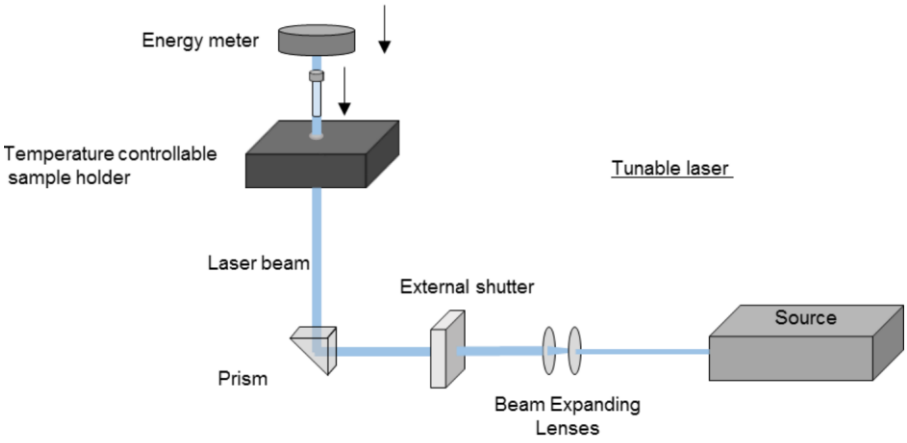

Figure S 6 Experimental setup for the tuneable laser experiments. Energy output is adjusted using an attenuator and read out with an energy meter before the sample is inserted into the sample holder.

2.2.1.2 CONTROL OVER INCIDENT PHOTON NUMBER[3]

The number of photons n_p ([n_p] = mol) that a monochromatic laser pulse contains can be calculated by application of the Planck-Einstein relation from the energy of the pulse E_{pulse}, the incident wavelength λ, Planck's constant h and the speed of light c.

$$n_p = \frac{E_{pulse} \ \lambda}{h \ c \ N_A} \qquad (2-2)$$

If the absorption of the glass vial and the extent of reflection and scattering at the vial at the respectively relevant wavelength is known, a target energy value can be calculated that must be reached during the above-described measurement to guarantee that the desired number of photons penetrates the sample solution during the subsequent irradiation. The wavelength dependent transmittance of the glass vials was determined experimentally using the above setup. Three glass vials were randomly selected as calibration vials. For varying wavelengths and in each case at a constant power output of the laser the energy was measured both with and without the calibration vials fitted into the sample holder. The top parts of these vials were cut off to minimize errors in the procedure, since only the bottom and sides of the glass vials would contribute significantly to the reduction of the photon flux that enters the solution.

The measured energy per pulse without a calibration vial in the sample holder is denoted as E_0 and the measured energy per pulse with a calibration vial in the sample holder as E_n. The transmittance was calculated as the ratio of E_n to E_0. The average transmittance over the measurements of the three vials (T_λ) was plotted together with the respective error (compare **Figure S 7**).

$$T_\lambda = \frac{E_n}{E_0} \qquad (2-3)$$

The target energy per pulse E_0 can be calculated directly from the wavelength λ, the number of pulses k, the transmittance of the glass vial at the respective wavelength T_λ and the desired total photon count n_p.

$$E_0 = \frac{n_\mathrm{p}\,\mathrm{N_A}\,\mathrm{h}\,\mathrm{c}}{k\,T_\lambda\,\lambda} \qquad (2-4)$$

By controlling the target E_0 at the respective wavelength, the number of photons that penetrate each sample solution of one set of experiments as described in the following subsections was guaranteed to be identical despite irradiation at different wavelengths.

2.2.1.3 Transmittance of Glass Vials

Transmittance of the bottom of the glass vials used in this study were obtained analogously to a method reported previously.[4]

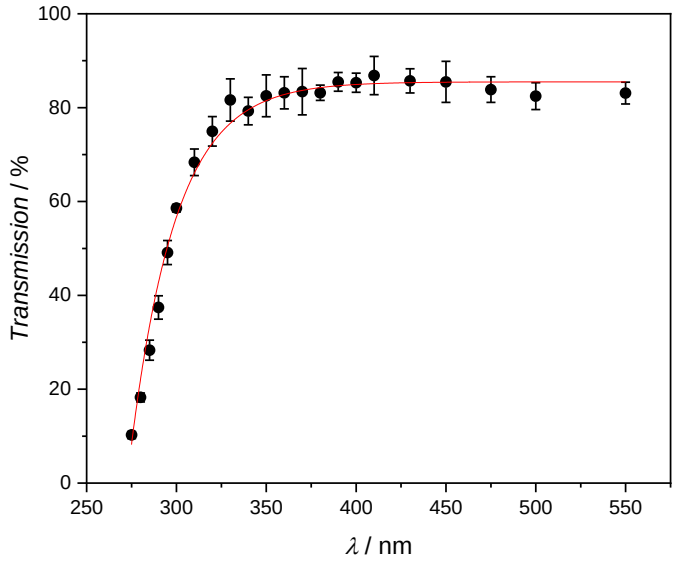

Figure S 7 Calibration of the glass vial transmittance including a fit to obtain values that were not determined experimentally.

2.2.1.4 SAMPLE PREPARATION FOR KINETIC MEASUREMENTS

APAT, *o*MBA and *N*-(2-hydroxy)ethyl maleimide were employed in a 1:1:8 ratio, with the total concentration being 0.5 mg mL^{-1} as per the LC-MS sample requirements. Sample solutions were freshly prepared every day and not kept overnight. Stock solution (APAT: 0.23 mM; *o*MBA: 0.23 mM; *N*HEM: 1.82 mM in MeCN) was prepared and degassed with N_2 for 15 min, then 0.3 mL were withdrawn and added to capped photo vials that had previously been degassed with N_2 for 5 min. The pathlength through the sample was ~10 mm. The samples were irradiated for the respective times, using the Coherent *Opolette* tuneable laser system and subsequently were filtered and directly used for LC-MS.

2.2.1.5 RESULTS OF LASER EXPERIMENTS

Table S 1 Detailed specifications of the laser experiments.

Wavelength / nm	Irradiation Time / min	Pulse Energy / µJ	Number of Photons / mol
320	0.1	500	1.17E-7
320	0.2	500	2.33E-7
320	0.4	500	4.86E-7
320	0.8	500	9.72E-7
360	1	500	1.50E-6
360	2	500	3.00E-6
360	4	500	5.99E-6
360	8	500	1.20E-5
360	19.3	500	2.89E-5
390	3.6	364	4.32E-6
390	7.2	364	8.65E-6
390	14.3	364	1.73E-5
390	28.6	364	3.45E-5
390	120	364	1.45E-4
450	5	2000	3.85E-5
450	10	2000	7.71E-5
450	15	2000	1.16E-4
450	30	2000	2.31E-4
450	156	2000	1.20E-3

2.2.1.6 LC-MS DATA PROCESSING AND CALCULATION OF PRODUCT YIELD

LC-MS chromatograms (scan wavelength 214 nm) were plotted and processed using Origin 2018 64Bit®. Chromatograms were baseline corrected and the peaks of APAT, CA_{APAT}, *o*MBA and CA_{oMBA} were integrated. A peak integral ratio *r* was calculated from the integrals by using the formulas:

$$r_{APAT} = \frac{I_{CA_{APAT}}}{I_{APAT} + I_{CA_{APAT}}} \qquad (2-5)$$

$$r_{oMBA} = \frac{I_{CA_{oMBA}}}{I_{oMBA} + I_{CA_{oMBA}}} \qquad (2-6)$$

If both the pyrazoline cycloadduct CA^{H}_{APAT} and the pyrazole cycloadduct $CA^{=}_{APAT}$ of APAT and *N*HEM were found, both were treated as one and the integrals were added up according to:

$$I_{CA_{APAT}} = I_{CA^{H}_{APAT}} + I_{CA^{=}_{APAT}} \qquad (2-7)$$

The difference in the molar absorption coefficients of APAT ($\varepsilon_{214\,nm}$ = 16900 (500) L mol^{-1} cm^{-1}), CA_{APAT} ($\varepsilon_{214\,nm}$ = 30200 (100) L mol^{-1} cm^{-1}), *o*MBA ($\varepsilon_{214\,nm}$ = 15700 (300) L mol^{-1} cm^{-1}) and CA_{oMBA} ($\varepsilon_{214\,nm}$ = 9400 (200) L mol^{-1} cm^{-1}) were then taken into account to calculate the yield. The numbers in brackets indicate the error obtained from the fit.

Each experiment was repeated 3x to obtain average yields and error bars.

Table S 2 Results of the laser experiments. Reaction conversion was determined *via* LC-MS. Error bars were obtained through 3x repetition of every experiment.

Wavelength / nm	Irradiation Time / min	Average Yield CA_{APAT} / %	Standard Error CA_{APAT} / %	Average Yield CA_{oMBA} / %	Standard Error CA_{oMBA} / %
320	0.1	0.0	0.0	23.0	0.4
320	0.2	0.0	0.0	38.0	0.7
320	0.4	0.0	0.0	66.4	0.9
320	0.8	0.0	0.0	89.0	1.5
360	1	0.4	0.0	9.0	0.4
360	2	0.6	0.3	16.4	2.9
360	4	0.7	0.4	32.2	3.8
360	8	2.3	0.4	59.7	0.8
360	19	4.3	0.2	91.2	0.3
390	3.6	0.7	0.0	1.0	0.2
390	7.2	1.4	0.0	2.1	0.2
390	14.3	2.8	0.5	4.5	0.6
390	28.6	4.5	0.1	9.1	0.1
390	120	21.1	2.8	45.4	1.1
450	5	5.7	0.1	0.0	0.0
450	10	10.8	0.4	0.0	0.0
450	15	14.7	0.5	0.0	0.0
450	30	32.0	0.8	0.0	0.0
450	156	86.2	3.4	0.0	0.0

2.2.1.7 DETERMINATION OF REACTION QUANTUM YIELDS

The reaction quantum yield was determined by measuring kinetics of the conversion over time (refer to **2.2.1.5**) and performing least squares fits of the experimentally determined conversions to the library of theoretical conversions simulated in Matlab®, (Eq. $(2-8)$-$(2-12)$) at each time interval. For a range of different values of the quantum yield Φ, using the starting concentration c(t0), the

molar absorptivity ε, the pulse energy Epulse and the wavelength □, the conversion after each laser pulse (n) was determined using the previous time step (n-1) by

$$c_{oMBA}(t_n) = c_{oMBA}(t_{n-1}) - \frac{E_{pulse}\lambda}{hc}\phi_{oMBA}10^{-\varepsilon_{oMBA}c_{oMBA}(t_{n-1})L} \quad (2-8)$$

$$c_{APAT}(t_n) = c_{APAT}(t_{n-1}) - \frac{E_{pulse}\lambda}{hc}\phi_{APAT}10^{-\varepsilon_{APAT}c_{APAT}(t_{n-1})L} \quad (2-9)$$

$$c_{NHEM}(t_n) = c_{NHEM}(t_{n-1}) - \frac{E_{pulse}\lambda}{hc}\phi_{oMBA}10^{-\varepsilon_{oMBA}c_{oMBA}(t_{n-1})L} - \psi\phi_{APAT}10^{-\varepsilon_{APAT}c_{APAT}(t_{n-1})L} \quad (2-10)$$

$$c_{CA_{oMBA}}(t_n) = c_{CA_{oMBA}}(t_{n-1}) - \frac{E_{pulse}\lambda}{hc}\phi_{CA_{oMBA}}10^{-\varepsilon_{oCA_{oMBA}}c_{CA_{oMBA}}(t_{n-1})L} \quad (2-11)$$

$$c_{CA_{APAT}}(t_n) = c_{CA_{APAT}}(t_{n-1}) - \frac{E_{pulse}\lambda}{hc}\phi_{CA_{APAT}}10^{-\varepsilon_{oCA_{APAT}}c_{CA_{APAT}}(t_{n-1})L} \quad (2-12)$$

Given the long irradiation times, diffusion was not taken into account in this simulation. A library of simulations, with quantum yield values varying between 0 and 1, was generated for each sample, using the parameters outlined in **Table S 3**. Least squares fitting of the simulation library to the experimental data was then performed to determine the best fit simulation, and hence quantum yield. The error of the quantum yield was calculated by propagation of the relative error of the absorption coefficients (obtained from concentration series and linear fitting) and the error of the least square fit of the simulation.

Table S 3: Quantum yield simulation parameters.

EXCITATION WAVELENGTH (nm)	320	360	390	450
E_{pulse} (J)	500×10^{-6}	500×10^{-6}	364×10^{-6}	2.00×10^{-3}
L (cm)	1.0			
$c_{OMBA}(t_0)$ (mol L^{-1})	0.23×10^{-3}			
$c_{APAT}(t_0)$ (mol L^{-1})	0.23×10^{-3}			
***N*HEM Equivalence**	7.9			

ε_{oMBA} (L mol^{-1} cm^{-1})	3340±20	87±3	3±1.5**	0
ε_{APAT} (L mol^{-1} cm^{-1})	6570±30	8920±50	9670±60	1720±10
ε_{NHEM} (L mol^{-1} cm^{-1})	418±2	32±1	0.6±0.3**	0
$\varepsilon_{CA,oMBA}$ (L mol^{-1} cm^{-1})	0	0	0	0
$\varepsilon_{CA,APAT}$ (L mol^{-1} cm^{-1})	9340±30	9920±30	10090±20	3150±10
***o*MBA QUANTUM YIELD (%)**	**18 ± 2**	**10 ± 2**	**20 ± 18****	*
APAT QUANTUM YIELD (%)	*	**(2.5 ± 0.5)x10^{-3}**	**(2.5 ± 0.5)x10^{-3}**	**(1.5 ± 0.5)x10^{-2}**

*Quantum Yield not determined due to negligible conversion

** Due to the low absorbance of the compounds at 390 nm, no absorption coefficient could be determined. Instead, it was assumed that absorbance is lowered by a factor of 10^{-3} compared to the respective absorption maximum. This value is highly uncertain, which is why the respective calculations have to be treated with great care. To account for the uncertainty, a relative error of ±50 % was assumed.

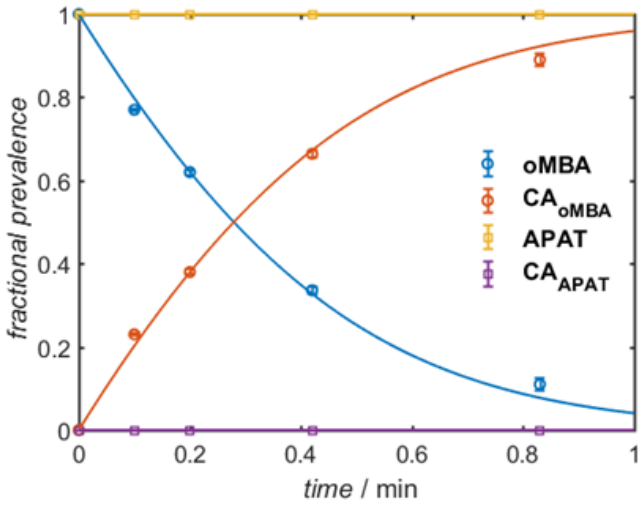

Figure S 8 Experimental time-dependent conversions (dots) of *o*MBA cycloaddition and APAT cycloaddition with *N*HEM in MeCN during irradiation with 500 µJ pulses of 320 nm, 20 Hz laser irradiation. Best-fit theoretical simulations used to determine reaction quantum yield are shown as solid lines.

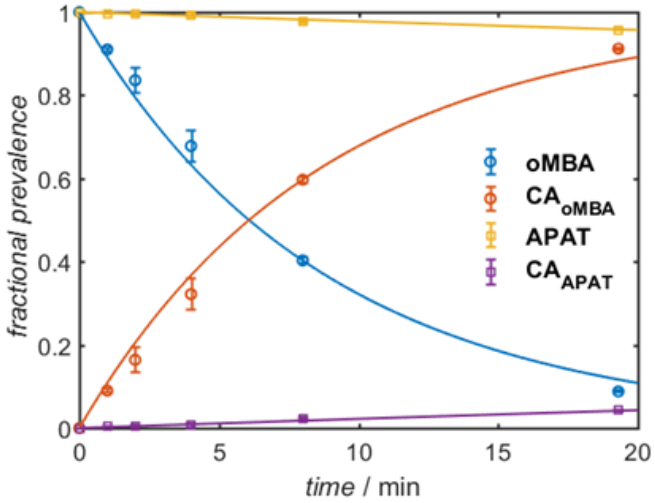

Figure S 9 Experimental time-dependent conversions (dots) of *o*MBA cycloaddition and APAT cycloaddition with *N*HEM in MeCN during irradiation with 500 µJ pulses of 360 nm, 20 Hz laser irradiation. Best-fit theoretical simulations used to determine reaction quantum yield are shown as solid lines.

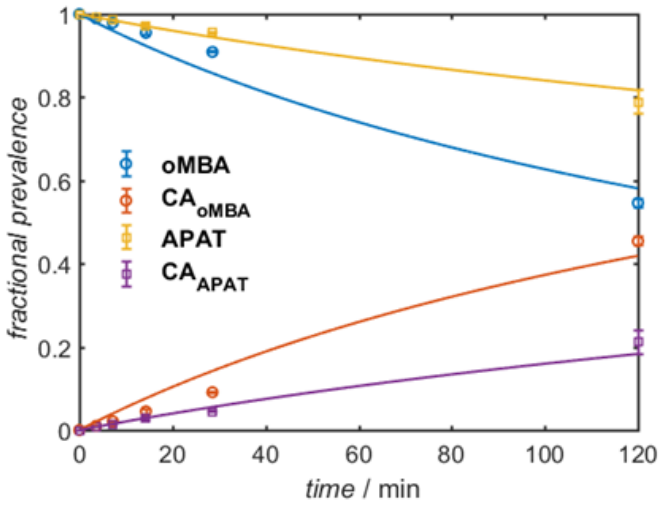

Figure S 10 Experimental time-dependent conversions (dots) of *o*MBA cycloaddition and APAT cycloaddition with *N*HEM in MeCN during irradiation with 364 µJ pulses of 390 nm, 20 Hz laser irradiation. Best-fit theoretical simulations used to determine reaction quantum yield are shown as solid lines.

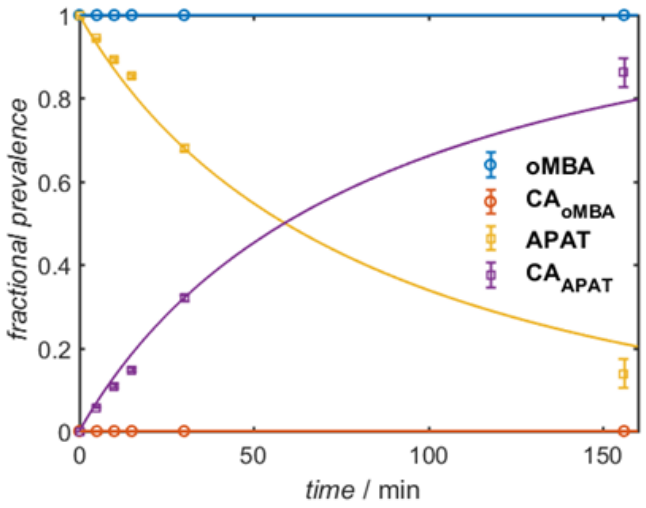

Figure S 11 Experimental time-dependent conversions (dots) of *o*MBA cycloaddition and APAT cycloaddition with *N*HEM in MeCN during irradiation with 2000 µJ pulses of 450 nm, 20 Hz laser irradiation. Best-fit theoretical simulations used to determine reaction quantum yield are shown as solid lines.

2.2.2 LED Experiments

2.2.2.1 Sample Preparation for Sequential LED Experiment

APAT, oMBA and *N*-(2-hydroxy)ethyl maleimide were employed in a 1:1:8 ratio, with the total concentration being 0.5 mg mL^{-1} as per the LC-MS sample requirements. The solution (APAT: 0.23 mM; *o*MBA: 0.23 mM; *N*HEM: 1.82 mM in MeCN, 15 mL total) was filled in a crimp vial, equipped with a stir bar, sealed and degassed with N_2 for 30 min.

2.2.2.2 Sequential LED Experiment

LED experiments were conducted using a Roithner LaserTechnik Gmbh DUV325-SD351 LED, which has emission centred around 325 nm, in addition to a ELE Doctor 10 W LED centered around 445 nm. The prepared sample vial was placed on top of the LED in 10 mm distance using a custom-made sample holder. The distance between sample and LED was kept small and constant, because the LED intensity significantly drops off at greater distances. A magnetic stirrer was positioned underneath to enable

stirring of the reaction mixture, and the LED was cooled using a compressed air flow (refer to **Figure S 12**). Samples were taken after the indicated time intervals (**Table S 4**), using a N_2-filled syringe.

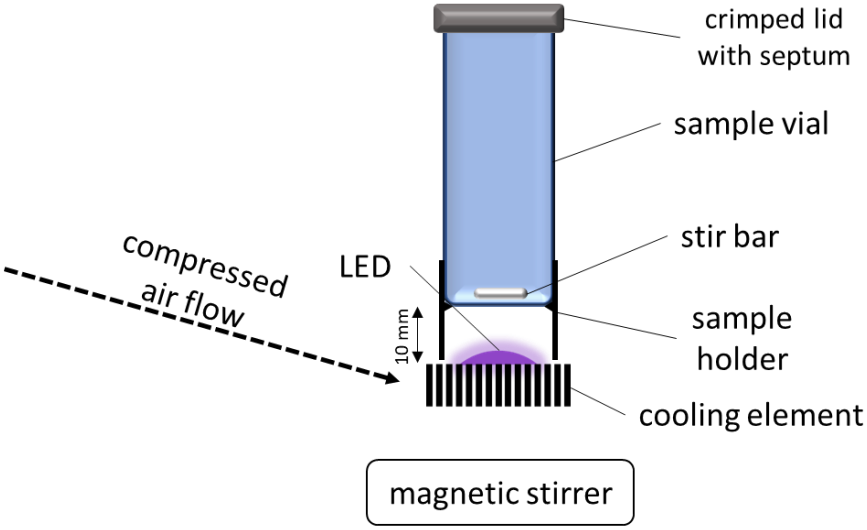

Figure S 12 Schematic setup of the LED experiment. The LED is placed below the vial and a fixed distance (10 mm) between sample vial and LED is ensured by a custom-made sample holder. The path length through the sample is ~4.5 cm.

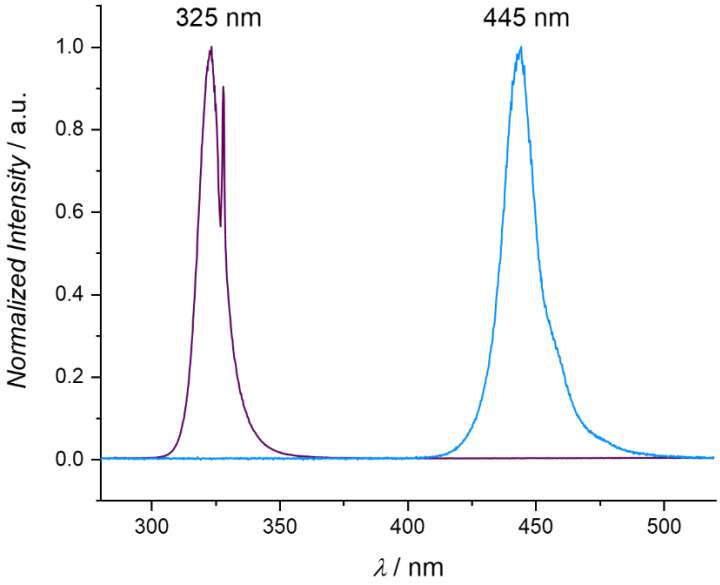

Figure S 13 Emission spectra of the two LEDs (325 nm, 0.67 W, FWHM = 13 nm and 445 nm, 10 W, FWHM = 18 nm)) used for the sequential LED irradiation experiment.

LED emission spectra were recorded using an Ocean Insight Flame-T-UV-Vis spectrometer, with an active range of 200-850 nm and an integration time of 10 ms. LED output energies were recorded using a Thorlabs S401C thermopile sensor, with an active area of 100 mm^2 and a wavelength range of 190 nm – 20 µm, connected to a Thorlabs PM400 energy meter console. The emitted power from each LED was measured for 60 seconds at a fixed distance (10 mm) from the sensor, after which the mean and standard deviation of the emission could be determined. LEDs were cooled during measurement to minimise any thermal effects on the emission power or sensor performance.

2.2.2.3 RESULTS OF THE SEQUENTIAL LED EXPERIMENT

The samples after irradiation were analyzed *via* LC-MS and quantified as described in 2.2.1.6.

Table S 4 Results of the sequential LED experiment. Reaction conversion was determined *via* LC-MS. Uncertainties of absorption coefficients were used to calculate errors.

Wavelength / nm	**Total Irradiation Time / min**	**Average Yield CA_{APAT} / %**	**Standard Error CA_{APAT} / %**	**Average Yield CA_{oMBA} / %**	**Standard Error CA_{oMBA} / %**
325	15	0.0	0.0	25.6	0.8
325	30	0.0	0.0	45.4	1.0
325	45	0.0	0.0	60.7	1.0
445	85	10.6	0.3	59.7	1.0
445	125	23.6	0.6	59.9	1.0
445	165	35.3	0.8	59.8	1.0
Dark	205	35.4	0.8	59.9	1.0
Dark	245	35.8	0.8	59.8	1.0
Dark	285	36.2	0.8	60.1	1.0
445	325	43.1	0.8	59.9	1.0
445	365	51.1	0.8	60.3	1.0
445	405	59.2	0.8	59.9	1.0
325	420	60.1	0.8	69.6	0.9
325	435	58.7	0.8	77.0	0.7
325	450	60.1	0.8	83.6	0.6

2.3 Isolation and Characterization of Photoadducts

2.3.1 CA_{APAT}

APAT (6 mg, 15.4 µmol, 1.00 eq.) and *N*HEM (17.4 mg, 123 µmol, 8.00 eq.) were dissolved in 35 mL MeCN in a round bottom flask, equipped with a stir bar and sealed with a rubber septum. The mixture was degassed by bubbling a stream of dried nitrogen for 1 h. The flask was then placed on a magnetic stirrer and a 10 W 445 nm LED was placed at an angle underneath the flask, so that the stir bar did not block the light. While stirring and cooling with a stream of compressed air, the mixture was irradiated for 16 h. Subsequently, it was passed over neutral aluminum oxide and purified by Puriflash silica column (gradient CH/EA 9:1 → 100 % EA). The solvent was evaporated, yielding 5.7 mg of a yellow solid (74 %).

^{1}H-NMR (600 MHz, toluene-d_8) δ [ppm] = 8.68 (m, 2H), 8.56 (d, J = 9.5 Hz, 1H), 8.47 (d, J = 9.5 Hz, 1H), 8.00 (d, J = 8.1 Hz, 1H), 7.89 (d, J = 8.2 Hz, 1H), 7.81 (d, J = 8.2 Hz, 1H), 7.78 (d, J = 8.8 Hz, 1H), 7.65 (d, J = 8.8 Hz, 1H), 7.46 (d, J = 8.2 Hz, 1H), 7.34 – 7.29 (m, 2H), 7.20 – 7.16 (m, 1H), 3.48 (t, 2H), 3.43 (t, J = 5.2 Hz, 2H), 2.72 (s, 6H).

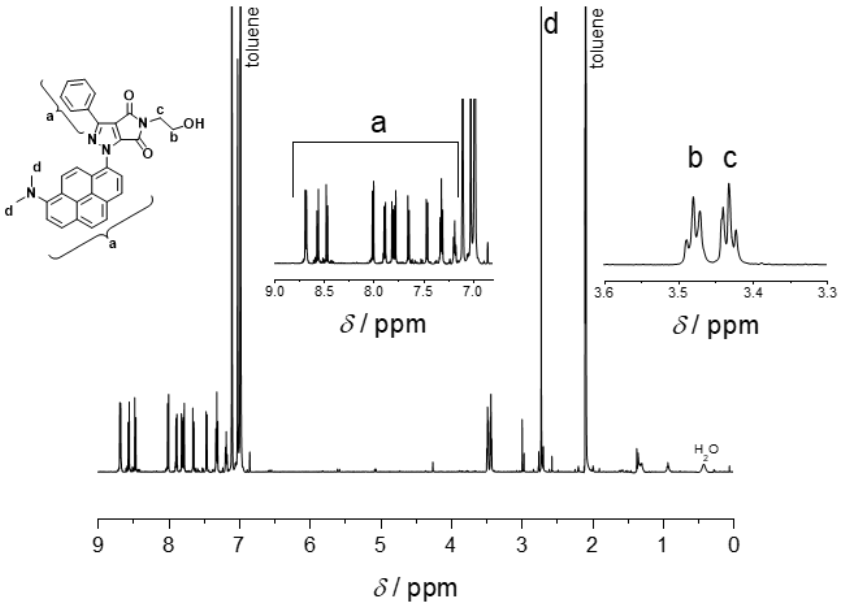

Figure S 14 ^{1}H-NMR spectrum of **CA_{APAT}** in toluene-d_8.

2.3.2 CA_{oMBA}

*o*MBA (10 mg, 66.1 µmol, 1.00 eq.) and *N*HEM (74.8 mg, 529 µmol, 8.00 eq.) were dissolved in 16 mL MeCN in a crimp vial, equipped with a stirring bar, and sealed. The mixture was degassed by bubbling a stream of dried nitrogen for 30 min. The vial was then placed on top of a 3 W 365 nm LED on a magnetic stirrer. While stirring and cooling with a stream of compressed air, the mixture was irradiated for 45 min. Subsequently, it was purified by Puriflash silica column (gradient CH/EA 9:1 → 100 % EA). The solvent was evaporated, yielding 11 mg of a white solid (57 %).

^{1}H NMR (600 MHz, MeCN-d_3) δ [ppm] = 7.08 – 6.94 (m, 1H), 6.72 – 6.58 (m, 2H), 5.48 – 5.34 (m, 1H), 3.61 (s, 3H), 3.47 – 3.26 (m, 4H), 3.11 (s, 1H), 3.02 – 2.75 (m, 3H), 2.75 – 2.56 (m, 2H).

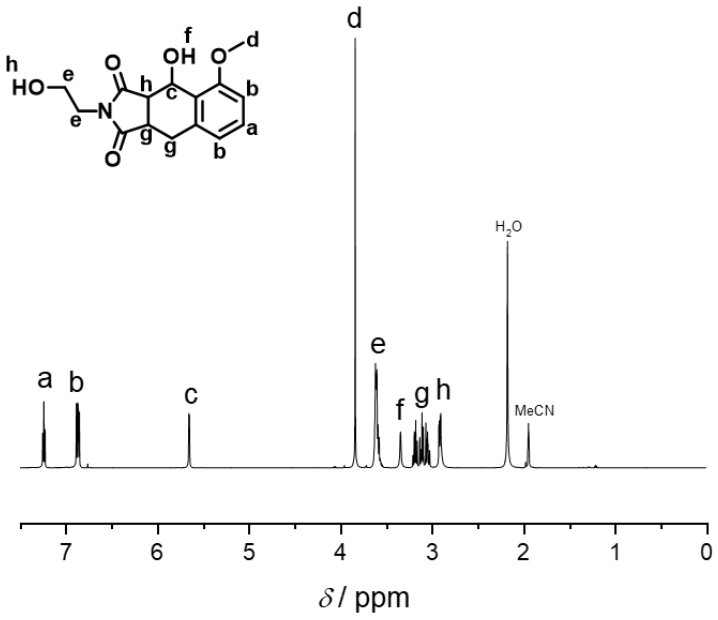

Figure S 15 ^{1}H-NMR spectrum of **CA_{oMBA}** in MeCN-d_3.

2.4 SYNTHESIS

2.4.1 MATERIALS

All chemicals were reagent or analytical grade and used as received, unless stated otherwise. 1-aminopyrene (97 %, Sigma-Aldrich), acetic acid (glacial, AJAX FineChem), acetic anhydride (analytical grade, Chem Supply), acetonitrile (HPLC grade, Chem Supply), aluminium oxide activated basic (for chromatography, Thermo Fisher Scientific), benzaldehyde (99 %, Sigma-Aldrich), chloroform (99.8 %, Thermo Fisher Scientific), chloroform-D ($CDCl_3$, 99.8 % D, + silver foil, Nova Chem), cyclohexane (ACS grade, Merck), dichloromethane (analytical grade, Thermo Fisher Scientific), dimethyl sulfoxide-D (DMSO-d6, 99.9 % D, Nova Chem), dimethylformamide (99.8 %, Sigma-Aldrich), ethanol (analytical grade, AJAX FineChem), hydrochloric acid (32 w%, Thermo Fisher Scientific), iodomethane (laboratory grade, Chem Supply), magnesium sulfate anhydrous (>98 %, Merck), methanol (analytical grade, Thermo Fisher Scientific), nitric acid (65 w%, Thermo Fisher Scientific), palladium on carbon (10 w%, Sigma-Aldrich), potassium carbonate anhydrous (analytical grade, Chem Supply), p-toluenesulfonyl hydrazide (97 %, Sigma-Aldrich), pyridine (99 %, Sigma-Aldrich), sodium chloride (analytical grade, Thermo Fisher Scientific), sodium hydrogen carbonate (analytical grade, Thermo Fisher Scientific), sodium nitrite (97 %, Thermo Fisher Scientific), sodium sulfate anhydrous (analytical grade, Thermo Fisher Scientific), tetrahydrofuran (HPLC grade, Thermo Fisher Scientific), toluene (analytical grade, Thermo Fisher Scientific), triphenylphosphine (99 %, Sigma-Aldrich).

Thin-layer chromatography (TLC) was performed on silica gel 60 F254 alumina sheets (Merck) and visualized by UV light. Column chromatography was run on an Interchim XS420 + SofTA Model 400 ELSD, or manually on silica gel 60 (0.04-0.06 mm, 230-400 mesh ASTM, Merck).

2.4.2 DIMETHYLAMINOPYRENE ARYL TETRAZOLE (APAT)

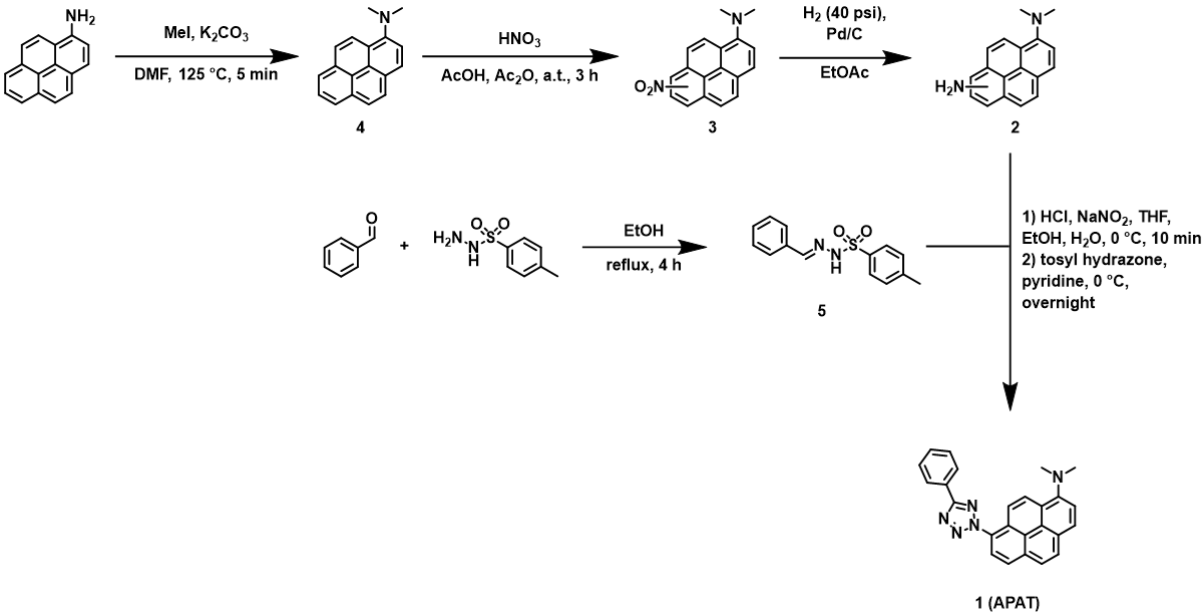

Scheme S 1 Summarized reaction route for the synthesis of APAT (**1**).

2.4.2.1 (*E*)-*N*'-BENZYLIDENE-4-METHYLBENZENESULFONOHYDRAZIDE (TOSYL HYDRAZONE) 5

A solution of benzaldehyde (1.00 g, 9.42 mmol, 1.00 eq.) and toluene sulfone hydrazide (1.75 g, 9.42 mmol, 1.00 eq.) in EtOH (20 mL) was refluxed for 4 h and subsequently poured into H_2O (100 mL). The precipitate was collected by filtration and dried in vacuum. The product was obtained as a white solid and used without further purification (2.55 g, 99%).

^{1}H-NMR (600 MHz, DMSO-d_6) δ [ppm] = 11.43 (s, 1H), 7.90 (s, 1H), 7.80-7.71 (m, 2H), 759-7.49 (m, 2H), 7.46-7.32 (m, 5H), 2.35 (s, 3H).

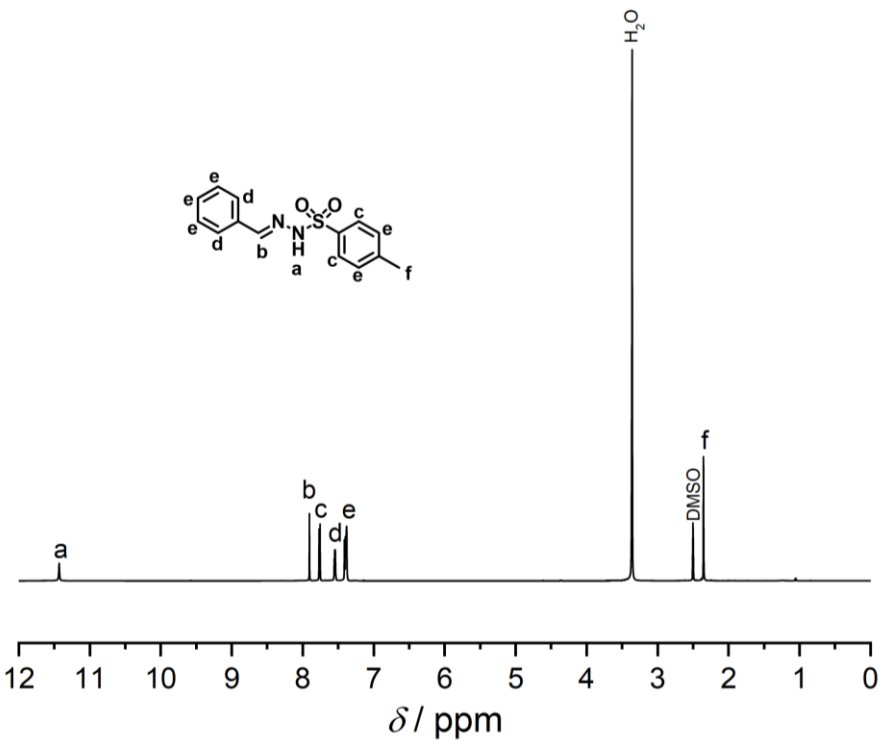

Figure S 16 ^{1}H-NMR spectrum of **5** in DMSO-d_6.

2.4.2.2 *N,N*-DIMETHYLPYREN-1-AMINE 4

Pyren-1-amine (4.96 g, 22.8 mmol, 1.00 eq.) and potassium carbonate (15.87 g, 114 mmol, 5.00 eq.) were combined in a round bottom flask and air was exchanged for argon. Dry DMF (30 mL) was added and, finally, iodomethane (7.11 mL, 16.2 g, 114 mmol, 5.00 eq.) was added dropwise over 10 min while stirring the brown solution. The flask was equipped with an argon filled balloon. Subsequently, the mixture was heated to 125 °C for 5 min and then allowed to cool down. Excessive iodomethane was quenched with 30 mL of MeOH, and the mixture was stirred for another 10 min. After ethyl acetate was added the mixture was extracted three times with water. The organic layer was dried over $MgSO_4$ and the solvent evaporated. The product was obtained as a brown oil and was used without further purification (5.27 g, 94 %).

^{1}H-NMR (600 MHz, $CDCl_3$) δ [ppm] = 8.48 (d, *J*= 9.2 Hz, 1H), 8.17-8.05 (m, 4H), 8.02-7.90 (m, 3H), 7.76 (d, *J* = 8.2 Hz, 1H), 3.07 (s, 6H).

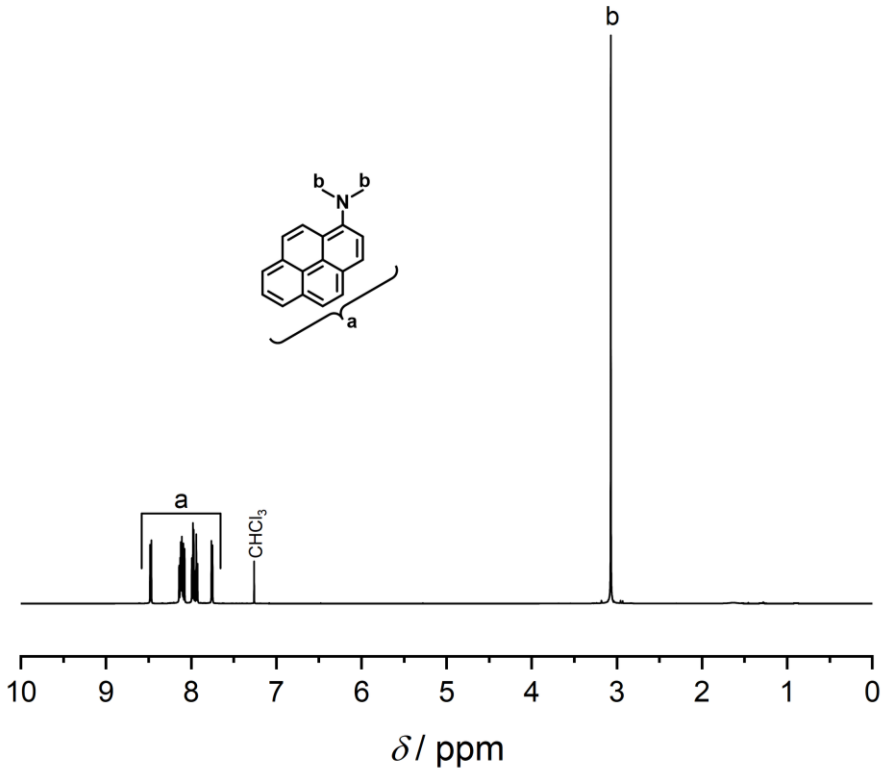

Figure S 17 ^{1}H-NMR spectrum of **4** in $CDCl_3$.

2.4.2.3 *N,N*-DIMETHYL NITROPYREN-1-AMINE 3

4 (3.53 g, 14.4 mmol, 1.00 eq.) was dissolved in acetic acid (200 mL) and acetic anhydride (55 mL). Under vigorous stirring, HNO_3 (1.68 mL, 65 w%, 2.37 g, 36.5 mmol, 1.70 eq.) in 10 mL AcOH was added dropwise over 1 h to the brown solution. TLC indicated presence of starting material (R_f = 0.7 in CH/EA 4:1) and mono-nitrated product (R_f = 0.5 in CH/EA 4:1). Another 0.3 eq. HNO_3 in 10 mL AcOH was added dropwise over an hour. This was repeated and each time the reaction was thoroughly monitored *via* TLC and ^{1}H-NMR spectroscopy to avoid formation of large amounts of double nitrated product. After a total amount of 2.5 eq. HNO_3 and 3.5 h reaction time, the mixture turned into a dark red and TLC indicated beginning formation of double nitrated product (R_f = 0.4 in CH/EA 4:1). The reaction was quenched with 150 mL H_2O. The mixture was extracted with chloroform four times and the organic layer washed with water twice, dried over $MgSO_4$ and filtered. The product was adsorbed onto Celite® filter agent and purified by column chromatography (silica, cyclohexane/ethyl acetate gradient (9:1 → 4:1 v/v)). Separation of regio-isomers was not achieved and the product contained *N,N*-dimethyl-8-nitropyren-1-amine, *N,N*-dimethyl-6-nitropyren-1-amine and *N,N*-dimethyl-3-nitropyren-1-amine in a ratio of 2:2:1, which was estimated from the relative peak integrals of the -NMe_2 signals in the ^{1}H-NMR spectrum. The product was obtained as a red powder (2.42 g, 58 %).

2.4.2.4 *N,N*-DIMETHYLPYRENE-1,8-DIAMINE 2

3 (2.36 g, 8.13 mmol) was dissolved in 130 mL ethyl acetate and Pd/C (692 mg, 10 w%, 650 μmol, 0.08 eq.) was added. After flushing with N_2 the vessel was filled with H_2 (40 psi) and shaken for 4 h. Over the course of the reaction, the mixture changed colour from dark red to blue with a yellow glint. The mixture was filtered over Celite® filter agent and the solvent was evaporated. The crude product was purified *via* Puriflash silica column (15 μm, cyclohexane/ethyl acetate gradient (99:1 → 4:1 v/v)). While the 1,3- and 1,6-substituted isomers were inseparable (R_f = 0.7 in CH/EA 1:1 v/v), a clean fraction of *N,N*-dimethylpyrene-1,8-diamine (R_f = 0.6 in CH/EA 1:1 v/v) was obtained. Position of the substituents was confirmed *via* NMR spectroscopy (^{1}H-NMR and ^{13}C-NMR spectroscopy, correlation spectroscopy (COSY), heteronuclear multiple bond correlation (HMBC) and heteronuclear single-quantum correlation spectroscopy (HSQC)). The product was obtained as a brown oil (861 mg, 41 %, R_f = 0.6 in CH/EA 1:1 v/v).

^{1}H-NMR (400 MHz, $CDCl_3$) δ [ppm] = 8.40 (d, *J*= 9.5 Hz, 1H), 8.02 (d, *J* = 8.2 Hz, 1H), 7.99-7.89 (m, 2H), 7.85-7.73 (m, 2H), 7.71 (d, *J* = 8.2 Hz, 1H)1 7.31 (d, *J* = 8.1, 1H), 4.29 (b, 2H), 3.05 (s, 6H).

^{13}C-NMR (150 MHz, $CDCl_3$) δ [ppm] =147.61, 140.49, 128.16, 126.77, 126.50, 125.96, 125.53, 125.07, 124.39, 123.80, 119.37, 117.36, 116.56, 113.91, 45.65.

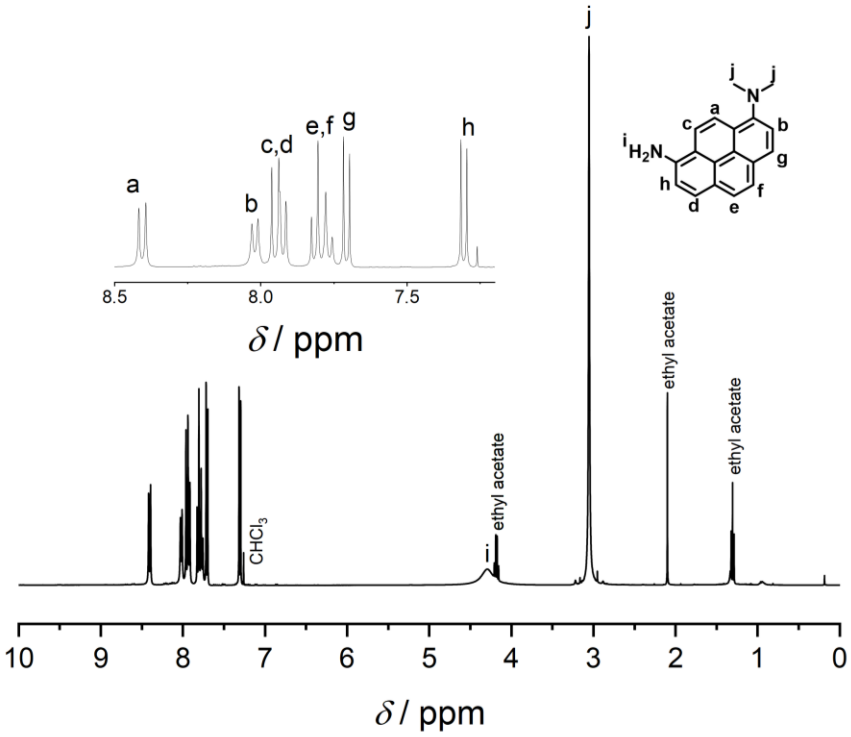

Figure S 18 ^{1}H-NMR spectrum of **2** in $CDCl_3$.

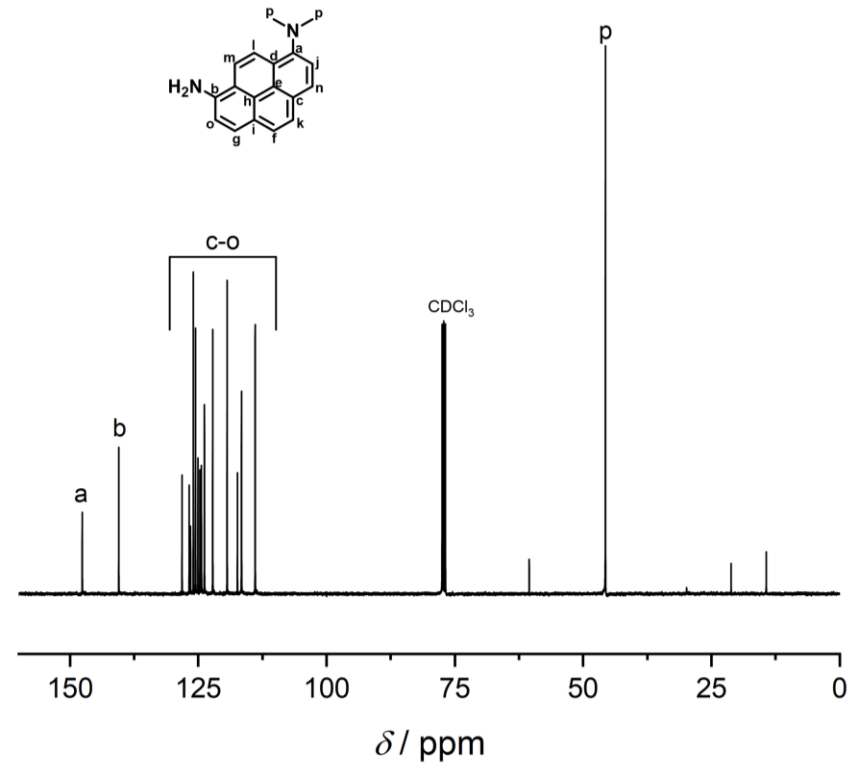

Figure S 19 ^{13}C-NMR spectrum of **2** in $CDCl_3$.

2.4.2.5 *N,N*-DIMETHYL-8-(5-PHENYL-2H-TETRAZOL-2-YL)PYREN-1-AMINE (APAT) 1

In a round bottom flask **2** (250 mg, 960 μmol, 1.00 eq.) was dissolved in a mixture of EtOH, H_2O (3 mL each) and HCl (294 μL, 37 w%, 3.46 mmol, 3.60 eq.) and cooled to -10 °C in an ice/salt mixture. In parallel, a solution of **5** (610 mg, 1.25 mmol, 1.30 eq.) in pyridine (6 mL) was prepared and likewise cooled to -10 °C. To the aqueous mixture was added $NaNO_2$ (66.3 mg, 960 μmol, 1.00 eq.) in a minimum amount of ice-cold water dropwise while vigorously stirring. The yellow mixture immediately turned dark blue and was continuously cooled and stirred for 10 min. Subsequently, the blue diazonium salt solution was quickly transferred to the cooled pyridine solution and the flask rinsed with 6 mL of cooled pyridine (-10 °C). The reaction flask was covered and allowed to warm up to ambient temperature overnight. Subsequently, the now red mixture was poured into 100 mL of 1M HCl and stirred for one hour. Ethyl acetate was added, and the product extracted and washed with H_2O until the aqueous layer was neutral. The organic layer was dried over Mg_2SO_4, filtered, and evaporated. The crude product was purified *via* Puriflash silica column (30 μm, cyclohexane/ethyl acetate gradient (99:1 → 95:1 v/v)). Finally, the product was recrystallized from MeCN to obtain a yellow powder (110 mg, 29 %, R_f = 0.7 in CH/EA 4:1 v/v).

^{1}H-NMR (600 MHz, $CDCl_3$) δ [ppm] = 8.58 (d, *J* = 9.6 Hz, 1H), 8.40-8.35 (m, 2H), 8.35-8.29 (m, 2H), 8.25-8.19 (d, *J* = 8.2 Hz, 2H), 8.12 (d, *J* = 8.9 Hz, 1 H), 8.00 (d, *J* = 8.8 Hz, 1H), 7.81 (d, *J* = 8.3 Hz, 1H), 7.62-7.51 (m, 3H), 3.09 (s, 6H).

^{13}C-NMR (150 MHz, $CDCl_3$) δ [ppm] = 165.45, 150.44, 133.54, 130.72, 129.39, 127.31, 12645, 125.03, 124.12, 122.96, 120.27, 117.36, 45.81.

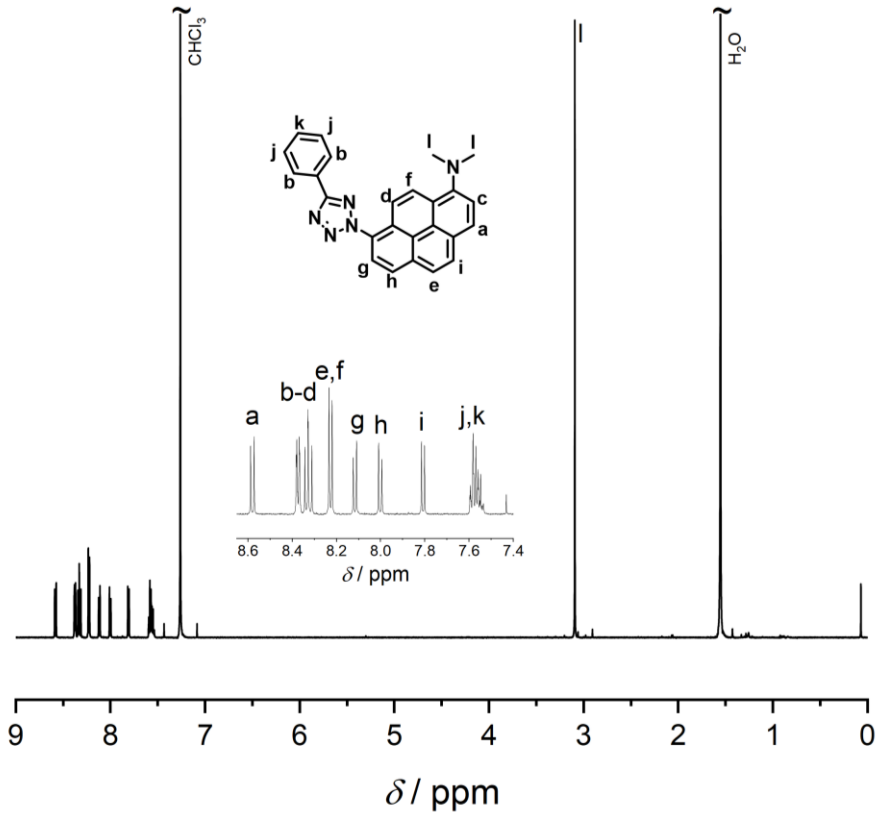

Figure S 20 ^{1}H-NMR spectrum of APAT (**1**) in $CDCl_3$.

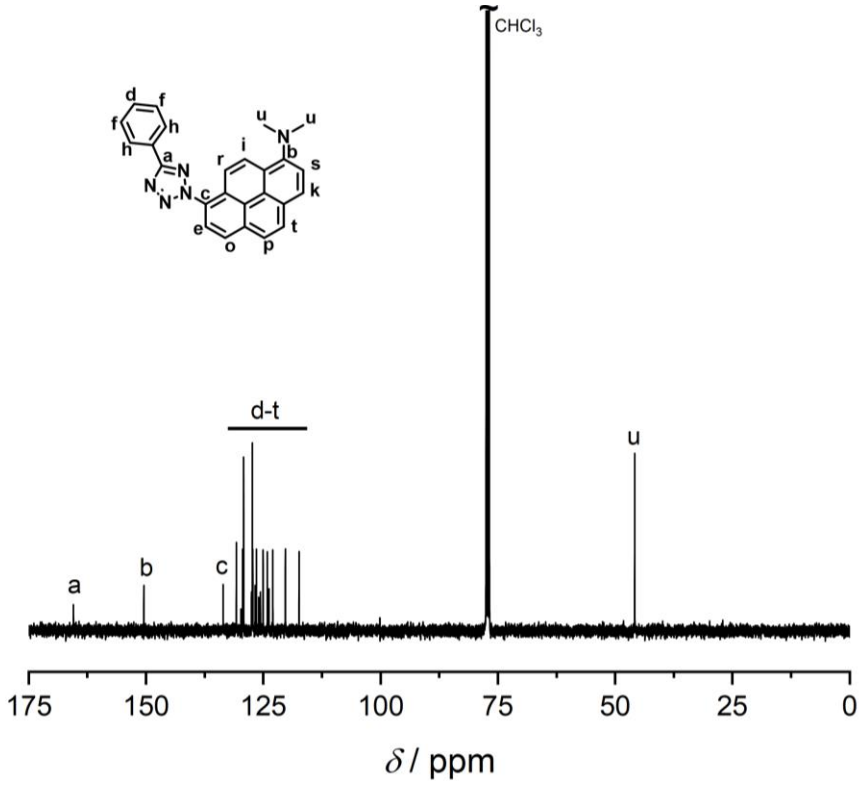

Figure S 21 ^{1}H-NMR spectrum of APAT (**1**) in $CDCl_3$.

2.4.3 2-METHOXY-6-METHYLBENZALDEHYDE

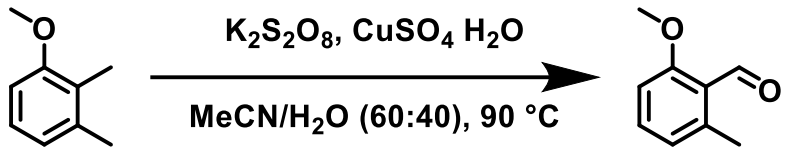

Scheme S 2 Synthetic route of 2-Methoxy-6-methylbenzaldehyde.

2,3-Dimethyl anisole (1 g, 7.34 mmol, 1.00eq.), copper sulfate pentahydrate (1.2 g, 7.49 mmol, 1.02 eq.) and potassium peroxodisulfate (5.95 g, 22.03 mmol, 3.00 eq.) were dissolved in 70 mL of water:acetonitrile (40:60) mixture. The suspension was stirred and refluxed at 90 °C for 60 min (thin layer chromatography (TLC) showed all the starting material had been consumed). The mixture was cooled to 0 °C using an ice-bath. The reaction mixture separated into a solid phase and two liquid phases. The liquid phases were decanted into a separating funnel. The aqueous phase was extracted three times with 100 mL DCM, the organic phases were combined, washed with brine, dried over Na_2SO_4 and the solvent was removed under reduced pressure. The crude product was sublimated under ambient nitrogen atmosphere at 85 °C to yield 0.91 g (82%) of colourless crystals.

^{1}H NMR (600 MHz, $CDCl_3$)(600 MHz, Chloroform-*d*) δ 10.64 (d, *J* = 0.7 Hz, 1H), 7.38 (dd, *J* = 8.4, 7.6 Hz, 1H), 6.87 – 6.78 (m, 2H), 3.89 (s, 3H), 2.57 (d, *J* = 0.7 Hz, 3H).

^{13}C NMR (151 MHz, Chloroform-*d*) δ 192.41, 163.28, 142.14, 134.55, 124.21, 123.46, 109.16, 55.89, 21.59.

LC-ESI-MS found $[M+H]^+$151.0753 (calculation $[M+H]^+$ 151.0754)

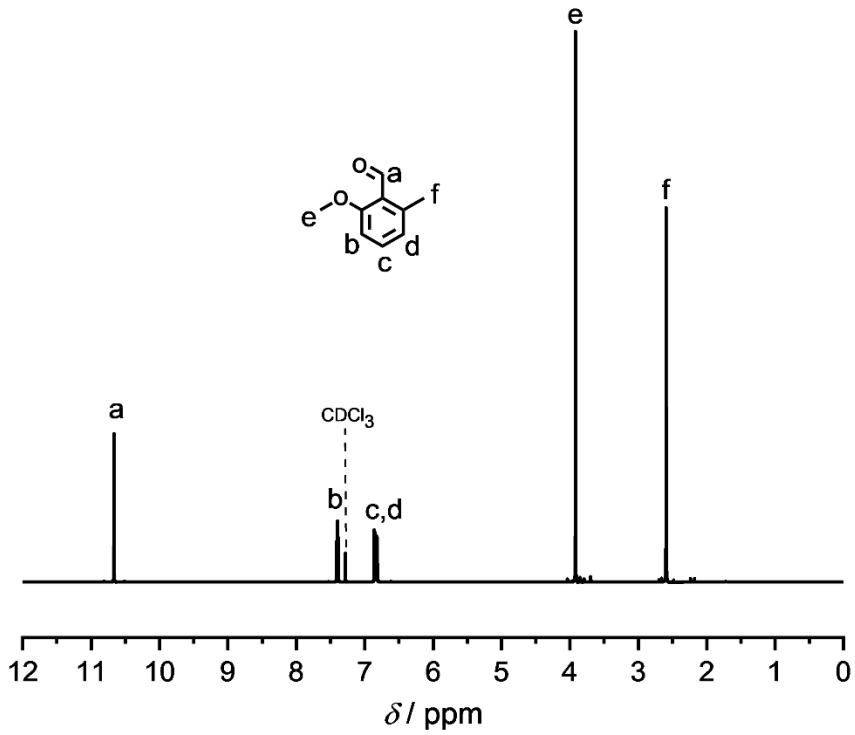

Figure S 22 ^{1}H-NMR spectrum of *o*MBA in $CDCl_3$.

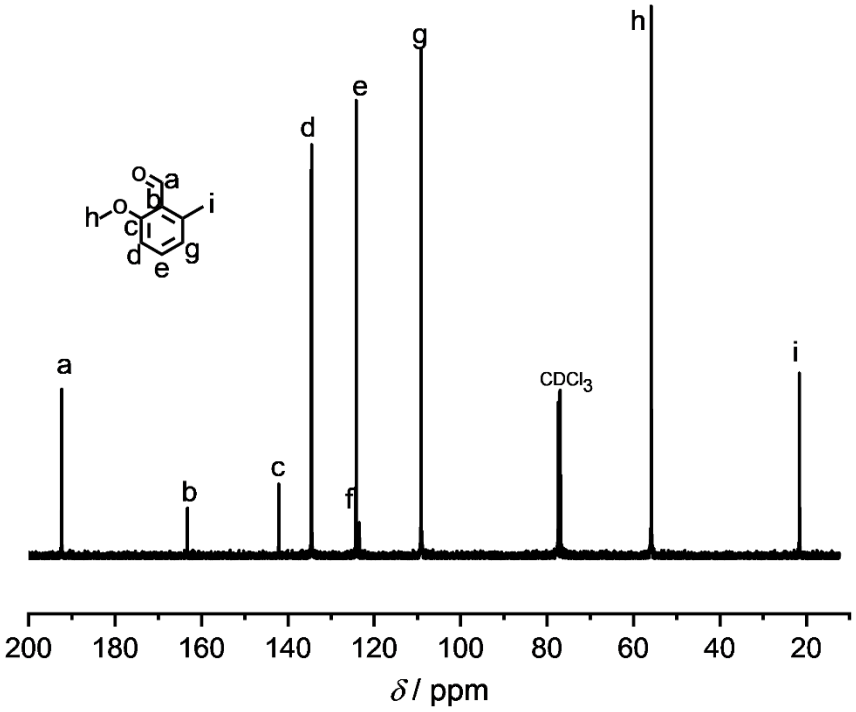

Figure S 23 ^{13}C-NMR spectrum of *o*MBA in $CDCl_3$.

3 SUPPORTING REFERENCES

1. Huisgen, R.; Sauer, J.; Seidel, M., Ringöffnungen der Azole, VI. Die Thermolyse 2.5-disubstituierter Tetrazole zu Nitriliminen. *Chemische Berichte* **1961,** *94* (9), 2503-2509.
2. Zheng, S.-L.; Wang, Y.; Yu, Z.; Lin, Q.; Coppens, P., Direct Observation of a Photoinduced Nonstabilized Nitrile Imine Structure in the Solid State. *Journal of the American Chemical Society* **2009,** *131* (50), 18036-18037.
3. Marschner, D. E.; Frisch, H.; Offenloch, J. T.; Tuten, B. T.; Becer, C. R.; Walther, A.; Goldmann, A. S.; Tzvetkova, P.; Barner-Kowollik, C., Visible Light [2 + 2] Cycloadditions for Reversible Polymer Ligation. *Macromolecules* **2018,** *51* (10), 3802-3807.
4. Menzel, J. P.; Noble, B. B.; Lauer, A.; Coote, M. L.; Blinco, J. P.; Barner-Kowollik, C., Wavelength Dependence of Light-Induced Cycloadditions. *Journal of the American Chemical Society* **2017,** *139* (44), 15812-15820.